Proceedings of the ASME 2011 International Design Engineering Technical Conferences & Computers and Information in Engineering Conference
IDETC/CIE 2011
August 29-31, 2011, Washington, DC, USA

DETC2011- 47713

AN XYZ PARALLEL KINEMATIC FLEXURE MECHANISM WITH GEOMETRICALLY DECOUPLED DEGREES OF FREEDOM

Shorya Awtar*, John Ustick, and Shiladitya Sen
Precision Systems Design Laboratory
Mechanical Engineering, University of Michigan
Ann Arbor MI 48109

ABSTRACT

We present the constraint-based design of a novel parallel kinematic flexure mechanism that provides highly decoupled motions along the three translational directions (X, Y, and Z) and high stiffness along the three rotational directions (θ_x, θ_y, and θ_z). The geometric decoupling ensures large motion range along each translational direction and enables integration with large-stroke ground-mounted linear actuators or generators, depending on the application. The proposed design, which is based on a systematic arrangement of multiple rigid stages and parallelogram flexure modules, is analyzed via non-linear finite element analysis. A proof-of-concept prototype of the flexure mechanism is fabricated to validate its large range and decoupled motion capability. The analyses as well as the hardware demonstrate an XYZ motion range of 10 *mm* x 10 *mm* x 10 *mm*. Over this motion range, the non-linear FEA predicts a cross-axis error of less than 3*%*, parasitic rotations less than *2 mrad*, less than 4*%* lost motion, actuator isolation less than 1.5*%*, and no perceptible motion direction stiffness variation. Ongoing work includes non-linear closed-form analysis and experimental measurement of these error motion and stiffness characteristics.

1. INTRODUCTION AND MOTIVATION

Flexure mechanisms derive motion from elastic deformation instead of employing traditional sliding or rolling interfaces [1-2]. This joint-less construction entirely eliminates friction, wear, and backlash, leading to highly repeatable motion [3]. Further benefits include design simplicity, zero assembly and maintenance, and potentially infinite life.

As a result of these attributes, flexure mechanisms are widely employed in various design applications. In particular, *multi-axis* flexure mechanisms are used in precision alignment and actuation instruments [4-5], MEMS sensors and actuators [6-7], energy harvesting devices [8], micro and nano manipulators [9], high dexterity medical devices [10], scanning probe systems for precision metrology and nanomanufacturing [11], as well as consumer products [12].

This multi-axis functionality may be achieved either via a serial kinematic [13-14] configuration or a parallel kinematic [15-17] configuration. While a serial kinematic design may be simply conceived by stacking one single-axis system on top of another until one achieves the desired degrees of freedom (DoF), this construction is often bulky, complex, and expensive. Moreover, moving cables and actuators adversely affect dynamic performance. Parallel kinematic designs, on the other hand, employ ground-mounted actuators and are often compact, simple in construction, and economical. Compared to serial kinematic designs, their main drawbacks include smaller motion range, potential for over-constraint, and greater error motions. Parallel kinematic designs are also not obvious and their conception presents a non-trivial design problem.

The key objective of this paper is to overcome the above-mentioned traditional drawbacks in the design of an XYZ parallel kinematic flexure mechanism. The proposed concept is inherently free of geometric over-constraints, resulting in large translational motions along the X, Y, and Z directions, and exhibits small error motions (cross-axis errors and parasitic rotations). Large motion range along multiple axes is critical in many of the above applications including nanopositioning and kinetic energy harvesting, which provide the primary motivation for this work.

Nanopositioning systems are macro-scale mechatronic motion systems capable of nanometric precision, accuracy, and resolution [18], and are therefore vital to scanning probe based microscopy, manipulation, and manufacturing [19-20]. Given their lack of friction and backlash, flexure mechanisms are the most common bearing choice for nanopositioning systems. However, most existing flexure-based multi-axis nanopositioning systems are capable of approximately *100* μm

* Corresponding Author (awtar@umich.edu, 734-615-0285)

motion range per axis (See prior art in *Section 2*). To broaden the impact of scanning probe techniques in nanometrology and nanolithography, there is a need to increase this motion range by several folds [21-23]. The challenge here lies not only in creating a multi-axis flexure mechanism that is capable of large motion range but also in the mechanical integration of the flexure bearing with ground-mounted actuators.

Since flexure mechanisms exhibit the motion guidance of mechanisms as well as the elastic attributes of structures, they are also highly suited for energy harvesting schemes based on a resonant proof mass subject to cyclic inertial loads. Even though the excitation, and therefore the available energy, is generally in multiple directions, most energy harvesting devices employ single axis resonators [24]. Given the fact that the energy harvested is directly proportional to the amplitude of oscillation [8], multi-axis flexure mechanisms with large motion range are very promising for efficient kinetic energy harvesting. In addition to providing large motion range in each direction, any candidate flexure mechanism also has to interface with fixed-axis linear or rotary generators for mechanical to electrical energy conversion.

In both these cases, a motion range of 10 *mm* per axis would be desirable in a macro-size construction. This paper covers the initial conception, analytical evaluation, and hardware validation of an XYZ parallel kinematic flexure mechanism that meets the large motion range requirement as well as the pertinent actuator/generator integration challenges associated with these applications. In *Section 2*, we describe these design challenges in addition to providing a brief overview of the existing literature on XYZ flexure mechanisms. In *Section 3*, we present the proposed XYZ flexure mechanism design along with a detailed description of its motion characteristics and a proof-of-concept hardware prototype. A comprehensive non-linear finite element analysis of this flexure mechanism design is presented in *Section 4*. The predicted motion performance in terms of motion range, cross-axis error, lost motion, parasitic rotations, and stiffness variation is reported. In *Section 5*, we discuss ongoing work in the design and fabrication of an experiment to validate the above motion characteristics, as well as a non-linear closed-form analysis to enable design optimization.

2. DESIGN CHALLENGES AND PRIOR ART REVIEW

Motion range in multi-axis parallel kinematic mechanisms is often restricted due to over-constraint, which can arise from a geometric layout that exhibits coupling between the motion axes. This ultimately leads to binding and restricts mobility. Thus, the motion axes – X, Y, and Z, in this case – must be sufficiently decoupled from each other so that motion in one axis does not affect or constrain motion in the other axes. Additionally, the undesired parasitic rotations (i.e., θ_x, θ_y, and θ_z) should be inherently restricted and minimized by the kinematics of the design. This eliminates the need for additional actuators, beyond the minimum three needed for X, Y, and Z actuation, to correct these undesired rotations. Moreover, in addition to providing geometric decoupling between the three motion axes, it is also important that the flexure mechanism addresses the geometric constraints associated with integrating practically available actuators or generators.

For an XYZ nanopositioning system, the use of linear actuators provides the greatest simplicity by avoiding any additional transmission. However, most linear actuators [25] – including voice coils, linear motors, piezoelectric stacks, and inchworm style actuators – produce motion along an 'actuation axis', defined by their geometry, and do not tolerate off-axis loads or displacements. Thus, for these actuators to be integrated with a multi-axis flexure mechanism in a nanopositioning system, it is critical that the point of actuation on the flexure mechanism be inherently constrained to move only along the direction of actuation. At the same time, this point of actuation should not be influenced by the actuation in other directions, and vice versa. This attribute is referred to as actuator isolation [26].

Similarly, most generators also have a fixed linear or rotary axis of motion defined by their geometry. This defined motion axis is essential for effective mechanical to electrical energy conversion, and therefore has to be accommodated in a parallel kinematic flexure mechanism designed for multi-axis energy harvesting.

Existing systematic and deterministic methods for the design of parallel kinematic flexure mechanisms [27-29] are limited to the study of motion between a ground and a motion stage, and do not address the additional geometric constraints associated with transducers. Also, these existing approaches do not recognize the benefits of elastic averaging [30] in flexure mechanisms, which can be leveraged to generate highly symmetric designs. Consequently, most existing parallel kinematic designs are based on qualitative arguments and rationale; a sampling of these designs is presented next.

Several macro-scale parallel kinematic XYZ flexure mechanisms have been reported in the literature but none provide the desired large motion range capability (~ 10 *mm* per axis). While some of these designs are true parallel kinematic arrangement, others represent a hybrid arrangement comprising a parallel connection of multiple serial kinematic chains.

In the former category, Davies [15] reports a three-DoF (XYZ) as well as a full six-DoF parallel kinematic design, with a sub-mm range per translational axis. Culpepper and Anderson [9] present a planar monolithic six-DoF compliant structure with a stroke of 100 μm per translational axis. Dagalakis et al. [16] offer a six-DoF hexapod type parallel kinematic design with improved actuator isolation. A six-DoF parallel kinematic stage is reported by Yamakawa et al. [31] that provides a 100 μm range in the X and Y directions, and 10 μm in the Z direction. Yet another XYZ design, with 140 μm range per axis, is presented by Li and Xu [32]. In all these cases, the motion range in each direction is primarily restricted due to inadequate geometric decoupling and/or actuator isolation between the multiple axes.

In the hybrid category, Yao et al. [17] use a parallel connection of three serial kinematic chains, each comprising

two four-bar parallelogram flexure mechanisms, to obtain X, Y and Z motion (85μm per axis) without any rotation. Arai et al. [33] also presents a spatial arrangement to achieve XYZ motion capability. Actuated by piezoelectric stacks, a motion range of 20 μm is reported. Similarly, Xueyen and Chen [34] employ a 3-PPP parallel mechanism to achieve good geometric decoupling and actuator isolation between the three motion directions. An overall motion range of 1 *mm* per axis is experimentally demonstrated. Another decoupled XYZ flexure mechanism design is conceptually proposed by Hao and Kong [35]. Here each of the three kinematic chains, which are connected in parallel, is individually a serial-parallel hybrid arrangement. While all these designs appropriately address the issues of geometric coupling and actuator isolation, their hybrid serial-parallel construction leads to a bulky and complex construction.

Apart from these macro-scale designs, several of multi-axis MEMS designs have also been reported for applications in inertial sensing and micro/nano manipulation [6-7, 36-38]. In this case, the designs and their associated performance are often dictated by the fundamentally planar nature of micro-fabrication. Given their small size, these designs generally exhibit a motion range of less than 10 μm per axis. However, since our focus in this paper is primarily on macro-scale devices and applications, we shall not delve further into these MEMS designs.

3. PROPOSED XYZ FLEXURE MECHANISM DESIGN

In this section, we propose a novel and compact parallel-kinematic XYZ flexure mechanism design that overcomes the above-listed challenges and meets the stated objective of large motion capability (~ 10 *mm*) and actuator/generator integration along each translational direction.

The proposed design, shown in Fig.1, is based on a systematic and symmetric layout of two kinds of building blocks – rigid stages and parallelogram flexure modules. The rigid stages are labeled as Ground, X stage, Y stage, Z stage, XY stage, YZ stage, ZX stage, and XYZ stage. This nomenclature is based on the primary mobility of any given stage – the X stage is constrained such that it has mobility along the X direction only, the XY stage is constrained such that it has mobility in the X and Y directions only, the XYZ stage is constrained such that it has mobility in the X, Y, and Z directions, etc. In the subsequent paragraphs, we describe how such mobility and constraint characteristics are achieved.

In addition to the rigid stages, there are 12 parallelogram flexure modules (PFM), which are grouped by color – green, blue, and red. The green PFMs, labeled G1 through G4, deform primarily in the X direction (Fig.1a) and remain stiff in all other directions; the red PFMs, labeled R1 through R4, deform primarily in the Y direction (Fig.1b) and remain stiff in all other directions; and, the blue PFMs, labeled B1 through B4, deform primarily in the Z direction (Fig.1c) and exhibit high stiffness in all other directions. Thus, the PFMs serve as constraint building-blocks, allowing certain motions and constraining others.

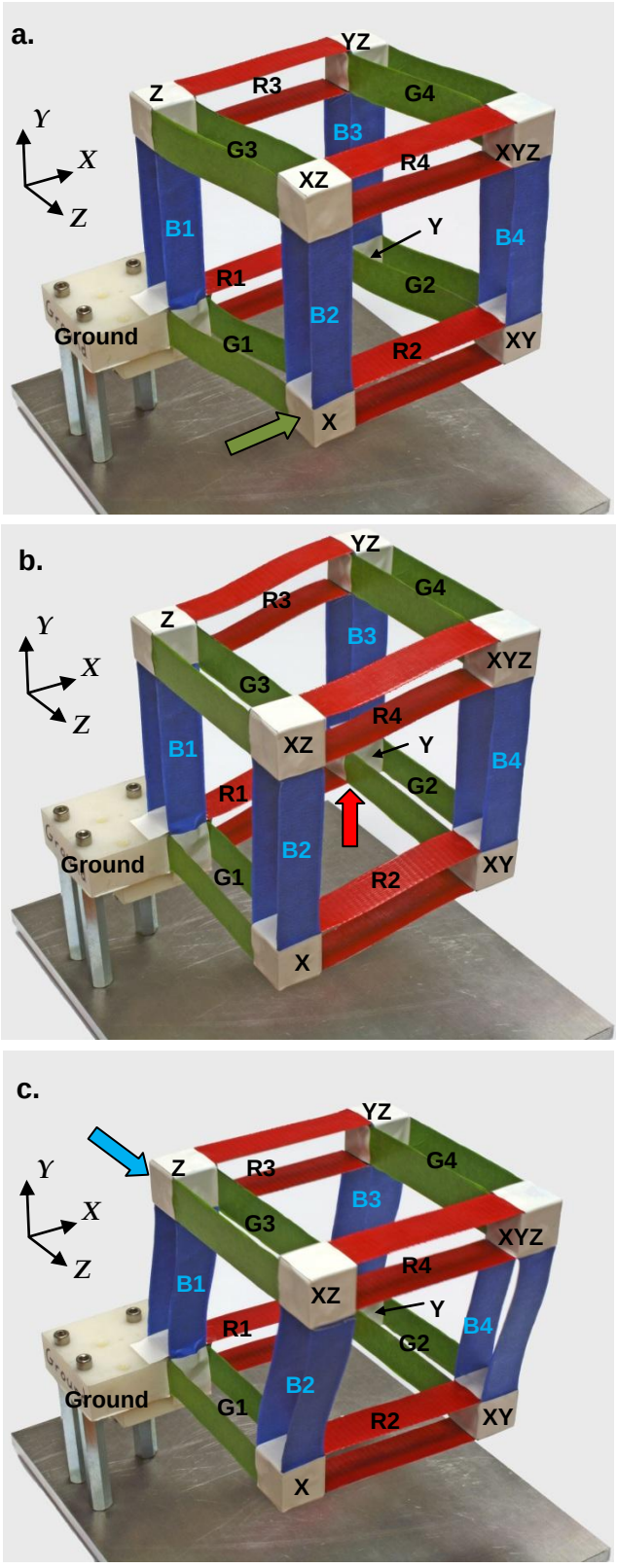

Fig. 1 Proposed Flexure Mechanism Design: A. X motion only B. Y motion only, C. Z motion only

As a consequence of this arrangement, the X stage is constrained to move primarily along the X direction guided by PFM G1, as seen in Fig.1a. Because of the high stiffness of the blue and red PFMs in the X direction, the X displacement of this X stage is passed on to the XY, XZ, and the XYZ stages. But at the same time, the XY and XYZ stage remains free to move in the Y direction because of the compliance of the red PFMs, and the XZ and XYZ stage remain free to move in the Z direction because of the compliance of the blue PFMs.

Similarly, the Y stage is constrained to move primarily along the Y direction because of PFM R1, as seen in Fig.2b. This Y displacement of the Y stage is transmitted to the XY, YZ, and XYZ stages because of the high stiffness of the green and blue PFMs in the Y direction. But at the same time, the XY and XYZ stage remain free to move in the X direction because of the compliance of the green PFMs, and the YZ and XYZ stage remain free to move in the Z direction because of the compliance of the blue PFMs.

Finally, the Z stage is constrained to move primarily along the Z direction because of PFM B1 (Fig.2c). This Z displacement of the Z stage is transmitted to the YZ, XZ, and XYZ stages because of the high stiffness of the green and red PFMs in the Z direction. But at the same time, the XZ and XYZ stage remain free to move the X direction because of the compliance of the green PFMs, and the YZ and XYZ stage remain free to move in the Y direction because of the compliance of the red PFMs.

A video demonstration of the motion characteristics of this XYZ flexure mechanism may be viewed here or may be requested from the authors. Thus, in principle, the X motion of the X stage is simply transmitted to the XYZ stage without affecting the latter's mobility in the Y and Z directions. By symmetry, a similar motion behavior is repeated in the other two directions as well. This inherent geometric decoupling between the X, Y, and Z axes produces large unconstrained motion along each individual direction.

Additionally, while the X stage is constrained to move primarily along the X direction, its motion does not influence the Y stage or Z stage. Again, due to symmetry, the same holds true for the Y stage and the Z stage. This unique behavior represents actuator isolation, which is critical to nanopositioning applications. Given this actuator isolation, the X stage, the Y stage, and the Z stage serve as the ideal locations to interface large-stroke fixed-axis linear actuators. In fact, the proposed parallel-kinematic flexure design behaves like a mechanical summation device – the X motion of the X stage, the Y motion of the Y stage, and the Z motion of the Z stage are all combined and exhibited at the XYZ stage. In a nanopositioning system, this XYZ stage would serve as the main motion stage with three-DoF.

This flexure mechanism is also ideal for multi-axis energy harvesting. Any arbitrary combination of the X, Y, and Z motions of the XYZ stage, which would serve as a proof mass in this case, gets mechanically separated into an X motion only at the X stage, a Y motion only at the Y stage, and a Z motion only at the Z stage. These single-axis motions can then be efficiently harvested using large-stroke fixed-axis linear generators.

To validate the above claims of unconstrained, decoupled, and large motions along the X, Y, and Z directions as well as actuator isolation, a proof-of-concept hardware prototype was fabricated (see Fig.1). The prototype qualitatively corroborates the predicted motion behavior, as can be viewed in the provided video.

At this point, we would like highlight the fact that the proposed design really represents a constraint map between rigid stages, wherein the parallelogram flexure module serves as a single translational DoF constraint. Instead, a multi-beam parallelogram, or a double parallelogram, or even a simple beam could have been employed as the constraint building block. This would result in a different XYZ flexure mechanism embodiment, however with the same geometric decoupling and actuator isolation behavior as seen above. For obvious reasons, error motions, stiffness variations, and dynamic behavior would be different.

In fact, if the constraint building blocks were to be ideal, i.e. zero stiffness in their DoF direction, and infinite stiffness and zero motions in their constrained directions, the resulting XYZ flexure mechanism would also be ideal – zero stiffness in the X, Y, and Z directions, zero parasitic rotations of the all the stages, perfect decoupling between the motion axes, perfect actuator isolation, zero lost motion between the point of actuation and the main motion stage, etc. However, in reality, any flexure module that is used as a constraint element is not ideal [39]. This gives rise to small but finite deviations of the resulting XYZ flexure mechanism from the ideal motion behavior.

With the feasibility of the proposed design established by means of a proof-of-concept hardware prototype, we next proceed to analytically determine the deviation of this design from ideal motion behavior. Of particular interest are the motion direction stiffness, cross-axis errors, transmission stiffness variation, lost motion, actuator isolation, and parasitic rotations [26, 39].

4. ANALYTICAL PREDICTION OF MOTION PERFORMANCE

The overall size, detailed dimensions, and material selection for the above-mentioned proof-of-concept hardware prototype were determined using a static failure (i.e. material yielding) criterion. Given the geometry and constraint pattern of the proposed design, it is evident that the constituent beam flexures deform predominantly in an S-shape. For this deformation, the maximum allowable end-deflection of a beam before the onset of yielding is given by [12]:

$$\Delta = \frac{1}{3}\cdot\frac{1}{\eta}\cdot\left(\frac{S_y}{E}\right)\cdot\left(\frac{L^2}{T}\right)$$

where η is the factor of safety, S_y is the yield strength, E is the Young's modulus, T is the beam thickness, and L is the beam length. For the material, we select Aluminum 6061 because of its overall good flexural properties and machinability. With this

choice, the desired XYZ stage motion range of 10 mm per direction (or Δ = +/– 5mm for individual beams) may be achieved with L = 101.6 *mm* (4 *in*) and T = 0.762 *mm* (0.030 *in*), while maintaining a safety factor (η) of 3. Using the subsequently presented analysis, we iteratively choose the beam width to be 25.4 *mm* (1 *in*) to minimize the stage rotations. This results in a center-to-center beam spacing of 24.64 *mm* for each parallelogram flexure module, and a 25.4 *mm* x 25.4 *mm* x 25.4 *mm* size for each of the rigid stages.

Having thus selected dimensions and material, we proceed to analyze the motion behavior of the proposed design in terms of its nonlinear force-displacement relations. The importance of geometric nonlinearities in the stiffness and error motion characteristics of beam flexures as well as flexure mechanisms constructed from beam flexures has been analytically and experimentally reported in the past [26, 39]. Ideally, a closed-form nonlinear analysis is preferable since it offers quantitative and parametric insight into the relation between the mechanism's geometry and its motion performance. However, such an analysis entails considerable mathematical complexity and is beyond the scope of this paper. Instead, to expediently obtain some early validation and assessment of the proposed design, we conduct a nonlinear finite element analysis (FEA) using ANSYS. Furthermore, this also helps highlight the extent of non-linear behavior in the mechanics of the proposed flexure mechanism design.

In the FEA, we model each beam in the flexure mechanism using a mesh of 100 BEAM 4 elements. The corner stages are modeled using the MPC184 rigid elements. To capture the pertinent nonlinearities, the consistent matrix and large displacement options (NLGEOM) are turned on and the shear coefficients are set to zero. Standard material properties for Aluminum 6061 are assumed (E = 68,900 $N.mm^{-2}$ and ν=0.33).

For the FEA, an X direction force (F_x^X**)** is applied at the X stage, a Y direction force (F_y^Y) is applied at the Y stage, and a Z direction force (F_z^Z) is applied at the Z stage. The forces in each direction are varied over a range of -29N to +29N in 11 equal increments, resulting in a total of 1,331 loading conditions that are analyzed. For each loading condition, the three translations and three rotations of each stage are recorded. For addressing these motions, we follow a nomenclature in which the super-script represents the rigid stage being considered and the sub-script represents the direction of displacement or rotation of this stage. For example,

U_x^X represents the X direction displacement of the X stage

U_y^X represents the Y direction displacement of the X stage

U_z^X represents the Z direction displacement of the X stage

θ_x^X represents the X direction rotation of the X stage

θ_y^X represents the Y direction rotation of the X stage

θ_z^X represents the Z direction rotation of the X stage

and so on…

In the subsequent paragraphs and plots, we present FEA results for the X direction only. Analogous motion behavior is seen in the Y and Z directions as well, due to the geometric symmetry of the proposed design, but is not presented here to avoid repetition.

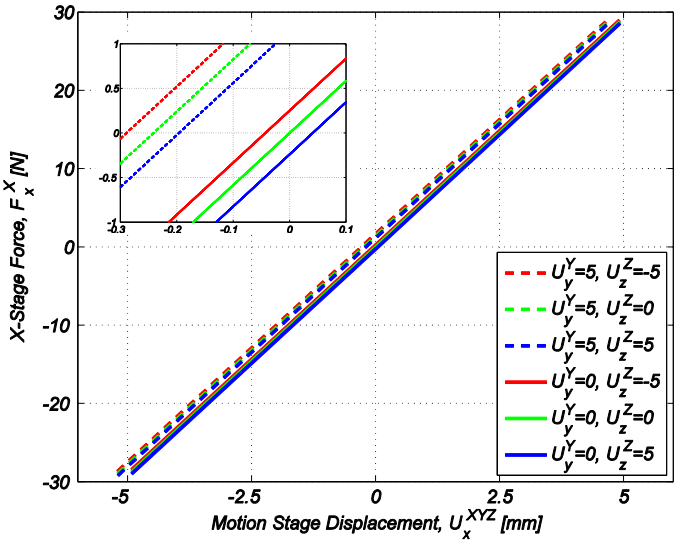

Fig.2 X Direction Force-Displacement Relation

Fig.2 illustrates the geometric decoupling between the X, Y, and Z motion directions in the proposed design. It plots the X direction force applied at the X stage (F_x^X) versus the X direction displacement of the XYZ stage (U_x^{XYZ}), for various combinations of Y and Z actuations (U_y^Y and U_z^Z). It is evident that the X direction stiffness not only remains constant over the entire X direction motion range, it is also insensitive to motions in the Y and Z directions. Although not plotted here, the Y and Z direction stiffness also exhibit a similar behavior. This validates the unique attribute of the proposed design that mobility in one direction is not influenced by motion in the other directions. This decoupling makes the design capable of large unconstrained motions (10 *mm*) in each direction.

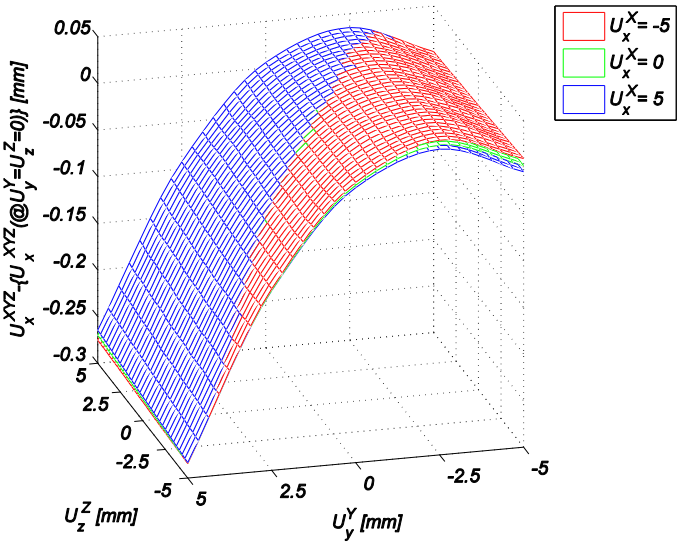

Fig.3 Cross-Axis Error Motion

Even though the X direction stiffness remains invariant in the presence of Y and Z direction actuation, a small shift in the plots can be seen in Fig. 2 (inset). This shift arises due to a combination of kinematic and elastic error motions in the constituent parallelogram flexure modules [39] and leads to a small cross-axis error in the overall flexure mechanism design. Cross-axis error represents any motion of the XYZ stage in one direction caused by actuation in a different direction. To highlight this error, we plot the difference between the actual X displacement of the XYZ stage (U_x^{XYZ}) in the presence of Y and Z actuation (U_y^Y and U_z^Z) and the nominal X displacement of the XYZ stage (U_x^{XYZ}) in the absence of Y and Z actuation. Thus, we plot $U_x^{XYZ} - \left\{U_x^{XYZ}\left(@U_y^Y = U_z^Z = 0\right)\right\}$ along the vertical axis for three different values of X actuation (U_x^X).

The three surface plots reveal that this cross-axis error has little dependence on the primary X actuation as well as the cross-axis Z actuation, but has a dominant dependence on the Y cross-axis actuation. This dependence has a kinematic quadratic component that arises from the arc-length conservation of the red PFMs in the presence of a Y direction displacement [39], and a linear component that arises due to elastic and elastokinematic effects in the blue and red PFMs.

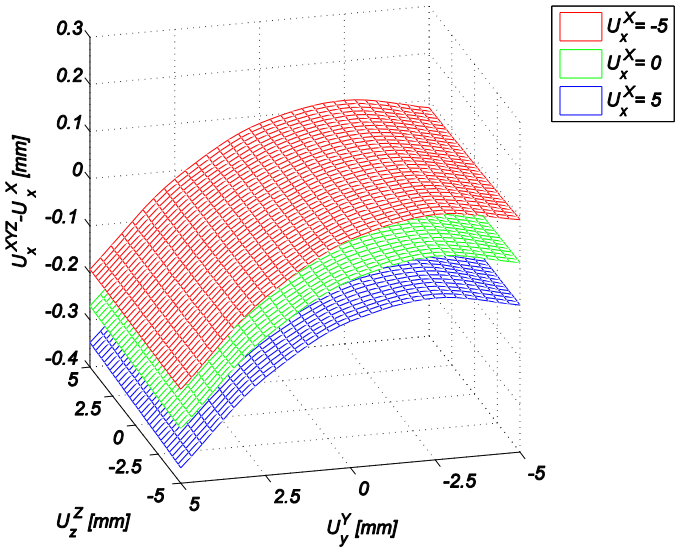

Fig.4 Lost Motion

Lost motion is the motion 'lost' between the point of actuation and the point of interest. Therefore, the difference between the X direction displacement of the XYZ stage (U_x^{XYZ}) and the X direction displacement of the X stage (U_x^X) constitutes the lost motion in the X direction. Lost motion should ideally be zero, but small deviations exist due to kinematic and elastokinematic effects [39] as shown in Fig.4. For three different values of the X actuation (U_x^X), the X direction lost motion is plotted over the entire range of Y and Z actuation (U_y^Y and U_z^Z). Lost motion is also inversely related to the transmission stiffness, which represents the stiffness between the point of actuation and point of interest and is critical in high speed motion control applications.

Actuator isolation in a multi-axis flexure mechanism ensures that the point of actuation in any given direction moves only in that direction and is not influenced by actuation in the other directions. The importance of actuator isolation in large-range nanopositioning was discussed in *Section 2*. Figures 5 and 6 show Z and Y direction displacement of the X stage (U_z^X and U_y^X), respectively. These motions are plotted for three different values of the X actuation (U_x^X) over the entire range of Y and Z actuation (U_y^Y and U_z^Z). The Z direction displacement of the X stage is primarily due to the kinematic arc-length conservation of the green PFMs, and therefore has a quadratic dependence on the X direction displacement of the X stage. The displacement of the X stage in the Y direction has a predominant dependence on the Z actuation, which arises due to the elastic error motion of the green PFMs [39].

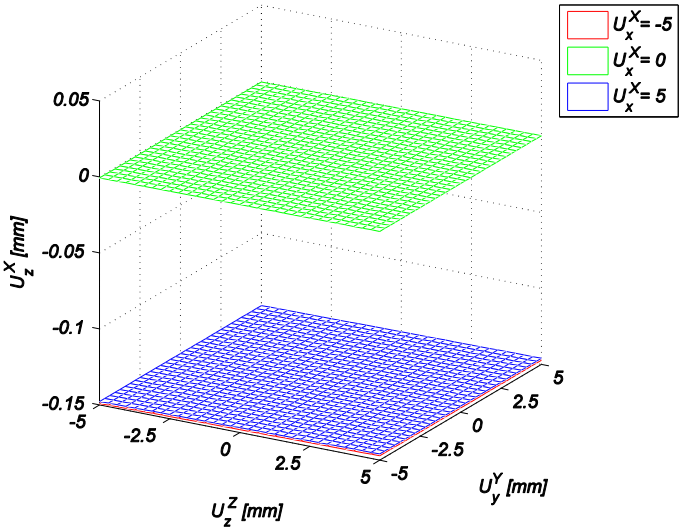

Fig.5 X Actuator Isolation (Z Direction)

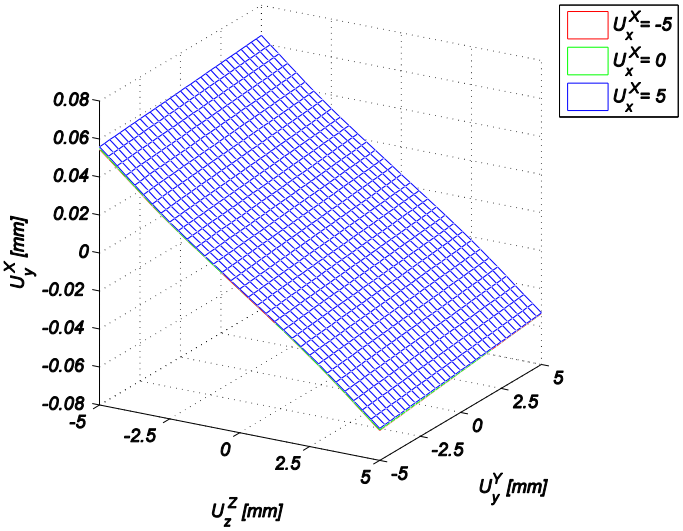

Fig.6 X Actuator Isolation (Y Direction)

In an XYZ flexure mechanism, all rotations are undesired and represent parasitic errors. Fig. 7 shows the XYZ-stage rotations about the X direction (θ_x^{XYZ}) over the range of X, Y, and Z stage displacements. The rotation varies primarily with the Y and Z actuation, which produce a twisting moment at the XYZ stage. Similarly, the XYZ stage rotation about the Y direction (θ_y^{XYZ}) depends on the X and Z actuation but not as much on the Y actuation. Furthermore, the XYZ stage rotation about the Z direction (θ_z^{XYZ}) depends on the X and Y actuation and not on the Z actuation.

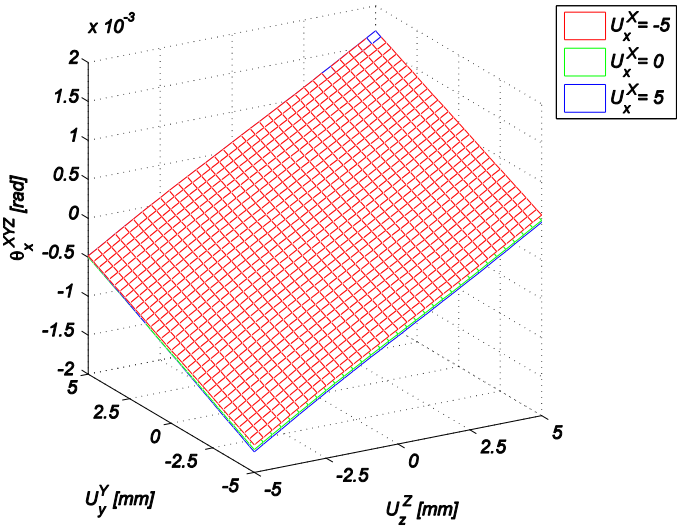

Fig.7 Motion Stage Rotation (about X Axis)

Below, we summarize the motion characteristics of the proposed XYZ flexure mechanism based on the above FEA results:

1. 10 *mm* motion range in each direction, with the stiffness remaining invariant with actuation along the other directions.
2. Cross-axis error less than 300 μm over the entire motion range (i.e. < 3%)
3. Lost motion per axis less than 400 μm over the entire motion range (i.e. < 4%)
4. Actuator isolation less than 150 μm in any given direction over the entire motion range (i.e. < 1.5 %)
5. Parasitic rotations of the XYZ stage less than 2 *milli-radians* over the entire motion range

6. CONCLUSION

We have proposed a novel, compact, and symmetric XYZ parallel kinematic flexure mechanism that provides highly decoupled motion along the three translational directions, inherently minimizes error motions, and accommodates large-stroke single-axis actuators/generators. These claims have been quantitatively validated via extensive finite element analysis and qualitatively demonstrated by means of a proof-of-concept prototype.

Because of its unique design, this flexure mechanism can be employed in an XYZ nanopositioning system to achieve an unprecedentedly large motion range in each direction. Although not highlighted in this paper, this flexure mechanism also enables large-range high-resolution multi-axis end-point sensing by resolving it into two simpler and practically realizable sensing tasks in each direction. High-resolution end-point sensing is indispensible in multi-axis nanopositioning.

Alternatively, the proposed flexure mechanism may be used as a resonant structure in an energy harvesting application to separate out the multi-axis motion of a proof mass into several individual single-axis motions. Large motion capability along multiple axes can lead to significant improvements in energy harvesting efficiency.

Our ongoing research efforts include a closed-form non-linear analysis of this flexure mechanism to gain greater design insight and to enable a parametric design optimization of its motion performance (e.g. maximize motion range, minimize error motions, etc.) for the above applications. We are also designing and fabricating an experimental setup to validate the predicted motion direction stiffness, cross-axis error, lost motion, actuator isolation, and parasitic rotations via direct measurements.

This research was supported in part by a National Science Foundation grant (CMMI # 0846738).

REFERENCES

[1] Jones, R. V., 1962, "Some uses of elasticity in instrument design," Journal of Scientific Instruments, 39

[2] Smith, S. T., 2000, *Flexures: Elements of Elastic Mechanisms*, Gordon and Breach Science Publishers,

[3] Slocum, A. H., 1992, *Precision Machine Design*, Society of Manufacturing Engineers, Dearborn, MI

[4] Chen, K. S., Trumper, D. L., and Smith, S. T., 2002, "Design and control for an electromagnetically driven X-Y-Θ stage," Precision Engineering, 26(4)

[5] Siddall, G. J., 1987, Flexure Stage Alignment Apparatus, US 4,694,477

[6] Ando, Y., 2004, "Development of three-dimensional electrostatic stages for scanning probe microscope," Sensors and Actuators A: Physical, 114(2-3)

[7] Mcneil, A. C., Li, G., and Koury, D. N., 2005, Single Proof Mass 3 Axis MEMS Transducer, US 6,936,492 B2

[8] Mitcheson, P. D., Rao, G. K., and Green, T. C., 2008, "Energy Harvesting From Human and Machine Motion for Wireless Electronic Devices," Proceedings of the IEEE, 96(9)

[9] Culpepper, M. L., and Anderson, G., 2004, "Design of a low-cost nano-manipulator which utilizes a monolithic, spatial compliant mechanism," Precision Engineering, 28(4)

[10] Awtar, S., Trutna, T. T., Nielsen, J. M., Abani, R., and Geiger, J. D., 2010, "FlexDex: A Minimally Invasive Surgical Tool with Enhanced Dexterity and Intuitive Actuation," ASME Journal of Medical Devices, 4(3)

[11] Du, E., Cui, H., and Zhu, Z., 2006, "Review of nanomanipulators for nanomanufacturing," International Journal of Nanomanufacturing, 1(1)
[12] Howell, L. L., 2001, *Compliant Mechanisms*, John Wiley & Sons
[13] Fischer, F. L., 1981, Symmetrical 3 DOF Compliance Structure, US 4,447,048
[14] Bednorz, J. G., Hollis Jr., R. L., Lanz, M., Pohl, W. D., and Yeack-Scranton, C. E., 1985, Piezoelectric XY Positioner, US 4,520,570
[15] Davies, P. A., 2001, Positioning Mechanism, US 6,193,226
[16] Dagalakis, N. G., and Amatucci, E., 2001, "Kinematic Modeling of a 6 Degree of Freedom Tri-Stage Micro-Positioner," Proc. ASPE 16th Annual Meeting
[17] Yao, Q., Dong, J., and Ferreira, P. M., 2008, "A novel parallel-kinematics mechanisms for integrated, multi-axis nanopositioning. Part 1. Kinematics and design for fabrication," Precision Engineering, 32(1)
[18] Hicks, T. R., and Atherton, P. D., 1997, *The Nanopositioning Book*, Queensgate Instruments Ltd.
[19] Application Note: Nanopositioning Tools and Techniques for R&D Applications, nPoint Inc
[20] Jordan, S., and Lula, B., 2005, "Nanopositioning: The Technology and the Options," The 2005 Photonics Handbook,
[21] Dai, G., Pohlenz, F., Danzebrink, H.-U., Xu, M., Hasche, K., and Wilkening, G., 2004, "Metrological large range scanning probe microscope," Review of Scientific Instruments, 75(4)
[22] Sinno, A., Ruaux, P., Chassagne, L., Topcu, S., and Alayli, Y., 2007, "Enlarged Atomic Force Microscopy Scanning Scope: Novel Sample-holder Device with Millimeter Range," Review of Scientific Instruments, 78(9)
[23] Wouters, D., and Schubert, U. S., 2004, "Nanolithography and nanochemistry: Probe-related patterning techniques and chemical modification for nanometer-sized devices," Angewandte Chemie International Edition, 43(19)
[24] Beeby, S., Tudor, M., and White, N., 2006, "Energy harvesting vibration sources for microsystems applications," Measurement Science and Technology, 12
[25] Smith, S. T., and Seugling, R. M., 2006, "Sensor and actuator considerations for precision, small machines," Precision Engineering, 30(3)
[26] Awtar, S., and Slocum, A. H., 2007, "Constraint-based Design of Parallel Kinematic XY Flexure Mechanisms," ASME Journal of Mechanical Design, 129(8)
[27] Blanding, D. L., 1999, *Exact Constraint: Machine Design Using Kinematic Principles*, ASME Press, New York, NY
[28] Hopkins, J. B., and Culpepper, M. L., 2010, "Synthesis of multi-degree of freedom, parallel flexure system concepts via Freedom and Constraint Topology (FACT) - Part I: Principles," Precision Engineering, 34(2)
[29] Su, H.-J., and Tari, H., 2010, "Realizing orthogonal motions with wire flexures connected in parallel," ASME Journal of Mechanical Design, 132(12)
[30] Awtar, S., Shimotsu, K., and Sen, S., 2010, "Elastic Averaging in Flexure Mechanisms: A Three-Beam Parallelogram Flexure Case Study," ASME Journal of Mechanisms and Robotics, 2(4)
[31] Yamakawa, K., Furutani, K., and Mohri, N., 1999, "XYZ-stage for Scanning Probe Microscope by Using Parallel Mechanism," Proc. ASME DETC 1999
[32] Li, Y., and Xu, Q., 2005, "Kinematic Design of a Novel 3-DOF Compliant Parallel Manipulator for Nanomanipulation," Proc. 2005 IEEE/ASME Advanced Intelligent Mechatronics
[33] Arai, T., Herve, J. M., and Tanikawa, T., 1996, "Development of 3 DOF micro finger," Proc. Intelligent Robots and Systems '96, IROS 96
[34] Xueyen, T., and Chen, I. M., 2006, "A Large-Displacement and Decoupled XYZ Flexure Parallel Mechanism for Micromanipulation," Proc. IEEE CASE 2006
[35] Hao, G., and Kong, X., 2009, "A 3-DOF Translational Compliant Parallel Manipulator Based on Flexure Motion," ASME IDETC 2009
[36] Li, F., Wu, M. C., Choquette, K. D., and Crawford, M. H., 1997, "Self-assembled microactuated XYZ stages for optical scanning and alignment," Proc. Solid State Sensors and Actuators, TRANSDUCERS '97
[37] Xinyu, L., Kim, K., and Sun, Y., 2007, "A MEMS stage for 3-axis nanopositioning," Journal of Micromechanics and Microengineering, 17(9)
[38] Sarkar, N., Geisberger, A., and Ellis, M. D., 2004, Fully Released MEMS XYZ Flexure Stage with Integrated Capacitive Feedback, US 6,806,991 B1
[39] Awtar, S., Slocum, A. H., and Sevincer, E., 2007, "Characteristics of Beam-based Flexure Modules," ASME Journal of Mechanical Design, 129(6)